CFD study on Spark Assisted Compression Ignition Combustion for a Natural Gas Powered Heavy Duty Engine

Federico Pessah

Abstract

Nowadays to have clean engines able to reduce both carbon dioxide and pollutants emissions is of fundamental importance for safeguarding and protecting the environment. For this reason, natural gas is a very interesting kind of fuel, since it does not form any particle matter and the low carbon-hydrogen ratio (C/H) leads to a reduced CO_2 production with respect to the combustion performed with the same amount of gasoline or diesel. Due to its high octane number, the thermodynamic cycle chosen as a reference is the "Otto cycle", but natural gas flame front velocity is not high enough to consider the combustion as instantaneous (which is the one theoretically assumed), especially in heavy duty engines where the displacement per cylinder can reach and overcome 2 liters. To do so, different and innovative combustion modes have been investigated using computational fluid dynamics: they all aim to exploit compression ignition, which in homogeneous charge context is faster with respect to flame propagation one, but far way more difficult to control. In this work, a spark assisted compression ignition engine has been simulated, highlighting advantages and drawbacks of this combustion mode and deriving some design criteria to develop this innovative kind of engine. At the end of the analysis, a pollutants emission computation has been performed, comparing carbon monoxide formation and unburnt fuel mass with values obtained by an entirely flame propagation combustion engine.

Introduction

Natural gas high octane number leads the engine manufacturers to develop a traditional Otto cycle, with a spark-plug installation at the centre of the head of the cylinder and to perform the combustion process through flame propagation in the whole volume.

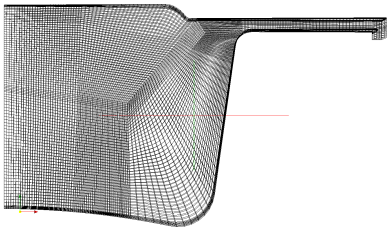

Figure 1: Mesh of the investigated engine

In figure 1, the combustion chamber of a typical heavy-duty natural gas powered engine is displayed. Injection system is a port fuel one, and charge can be assumed homogeneous. When dealing with heavy duty application (where displacements per cylinder can easily overcome the value of 2 liters), path to be covered by the flame is considerable, and hence knock occurring probability is enhanced. This is the reason why even if octane number of natural gas is very high (in the range between 120 and 130 even if not strictly defined), compression ratio adopted in the engine is limited, affecting performance and fuel consumption. At the same time, a well-exploited spontaneous ignition can lead to adopt higher compression ratios and a faster combustion at the same time, but it is very difficult to control and it can induce very severe loads to the mechanical structure of the engine. Therefore, as first choice HCCI (homogeneous charge compression ignition) engines were developed, working with huge air excess (equivalence ratio ϕ between 0.5-0.6) and gasoline or natural gas used as fuels, ignited entirely by compression. This combustion mode theoretically was leading to enormous efficiency improvements, but in practice it generated very violent pressure waves

inside the cylinder and combustion was very difficult to control. These are the reasons why researchers switched to spark assisted compression ignition (SACI) combustion, where a part of the mixture was supposed to burn due to flame propagation and the remaining one to autoignite spontaneously. This last combustion mode can not permit such a high compression ratio as in HCCI engines, but the presence of the spark-plug leads to have a better control to the combustion process itself, especially to not induce too high loads to the engine. In addition, this consideration is fundamental especially when natural gas is chosen as a fuel: its octane number is not commercially defined, and autoignition strength can vary regions by regions depending on the kind of natural gas composition used. Therefore, it is fundamental to detect and clearly define the difference between knock and a well-exploited spontaneous ignition, and then to use the obtained results to develop a spark assisted compression ignition engine.

Objectives

Objective of this investigation is to verify that this combustion mode can take some efficiency advantages to the engine: ideal Otto cycle combustion is instantaneous, but flame propagation one can last even 50 CAD of engine time. In addition, a well exploited spontaneous ignition leads to the possibility to adopt higher compression ratio, increasing even more the theoretical thermal efficiency of the cycle. Simulation setup chosen is a 2D mesh, with axial symmetry imposed for the whole combustion chamber. Some important design criteria to have a good exploitation of the SACI (spark assisted compression ignition) combustion mode have been derived investigating piston shape and air-fuel ratio.

Solver setup

This investigation has been carried out by building a solver in OpenFOAM® environment, in order to use all the utilities available from the open-source software and to build a code suitable for the illustrated objectives at the same time. The algorithm must hence consider both kinds of combustion modes present in the engine: flame propagation has been computed exploiting the Weller combustion model, while spontaneous ignition has been simulated using tabulated kinetics with the help of Cantera®. In both cases, two different progress variables are introduced: c and c_{fresh}. A progress variable is a specific quantity implemented in the CFD solver which is initialized at 0 having a monotonous trend up to 1:

$$\begin{array}{c}\text{Progress variable}\\ 0 \longrightarrow 1\end{array}$$

As the name suggests, they are introduced to indicate the combustion progress: they assume the value of 0 if no reaction occurred, while they reach the value of 1 whenever combustion can be considered entirely completed. Therefore, a thermodynamic quantity which has this behavior must be chosen: during this work, c is the species formation enthalpy at a reference temperature of 298 K, as it has a monotonous trend with the combustion process from a minimum up to a maximum value. To make it from 0 to 1, the progress variable has been normalized:

$$c_{Norm} = \frac{h - h_{min}}{h_{max} - h_{min}} \tag{1}$$

In this way, consistency between combustion chemical reactions and heat released by them is guaranteed. Therefore, the following implementation has been chosen:

- c for flame propagation combustion

- c_{fresh} for compression ignition combustion

The two phenomena by a solver point of view are clearly detached, and they can not interact one with the other. As explained in "The Development of a New Flame Area Combustion Model Using Conditional Averaging" published by H.G. Weller in 1993, flame propagation combustion model is written with respect to the regress variable b, to have considerable numerical advantages:

$$b = 1 - c_{Normalized} \tag{2}$$

$$\nabla b = -\nabla c_{Normalized} \tag{3}$$

There is no strong conceptual difference between b and c, but the former is initialized to 1 and proceeds to 0 as combustion takes place: for this reason, b

is named "regress variable". To have a good representation of the flame, its velocity is computed cycle per cycle, hence also Ξ is initialized:

$$\Xi = \frac{A_f}{A_s} = \frac{S_{turbulent}}{S_{laminar}} \tag{4}$$

This Ξ is derived by the ratio of vortex normal vector with respect to surface front one, but as illustrated in equation 4 it can be easily re-conduced to the ratio of the flame front turbulent velocity with respect to the laminar one. With this settings the two equations model can be implemented:

$$\frac{\partial \rho b}{\partial t} + \nabla \cdot (\rho \vec{u} b) - \nabla \cdot (\mu_t \nabla b) = \rho \vec{u} S_u \Xi |\nabla b| \tag{5}$$

An algebraic expression was used to compute Ξ. Spontaneous ignition instead must be considered in a completely different way, because there is not a reaction front propagating inside the combustion chamber; at the same time, the number of possible oxidation reactions for every kind of hydrocarbon are in the order of magnitude of hundreds or thousands, so in terms of computational time it would result too expensive to implement all of them. Therefore, the concept of autoignition delay has been exploited: for every pressure, temperature and mixture fraction conditions, a quantity of time is necessary for spontaneous ignition to occur. This delay time can be evaluated using an Arrhenius correlation:

$$\tau_a = A p^{-n} exp(\frac{E_a}{RT}) \tag{6}$$

In the equation 6 it is possible to appreciate how high cylinder temperatures enhance spontaneous ignition massively, as autoignition delay trend with temperature is exponential. Even for this reason, fresh unburnt specific quantities must be numerically detached by flame propagation ones, as in combustion chambers at the same time unburnt gases temperatures are about 1000 K while burnt ones have a typical temperature value of 2600 K in stoichiometric mixture conditions. Therefore, even before the simulation a table of kinetic chemistry is generated, as illustrated in figure 2.

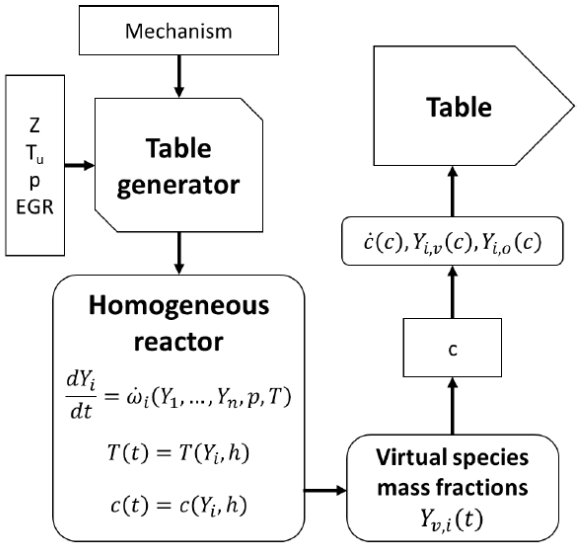

Figure 2: Tabulated kinetic computation for every fuel

Before the simulation, a set of different pressures (p), temperatures of unburnt charge (Tu), mixture fractions (Z) and exhaust gas recirculation (EGR) must be provided to the mechanism, which computes the chemical reaction velocity rate for every combination of them. Since no exhaust gas recirculation is considered in this work, the size of the table is going to be:

$$N_{table} = n_p \cdot n_{Tu} \cdot n_Z \tag{7}$$

Where n stands for the number of input values for any specific quantity. In natural gas powered engines compression ratios are high with respect to the other spark ignition thermal machines, and also due to the presence of the temperature gradient generated by the flame, T_u maximum to be assumed must be high. As this table is generated before the simulation, it is not possible to have a precise knowledge of maximum unburnt temperature value, but if it is underestimated the whole computed results are compromised; otherwise, if Tu is overestimated, there will be just an increase of computational time needed for the table generation. Once provided the described inputs, the mechanism returns as output different values of $\dot{c}_{fresh}$, the compression ignition progress variable source term. In the end, the following combustion

transport equation can be written:

$$\frac{\partial \rho c_{fresh}}{\partial t} + \nabla \cdot (\rho \vec{u} c_{fresh}) + \mu \nabla c_{fresh} = \rho \dot{c}_{fresh} \cdot b \tag{8}$$

Equation 8 reports on the left side time-derivative, convection and diffusion term as every conservation equation; on the right side the source term related of progress variable increasing, composed by:

- a term proportional to chemical reactions velocity ($\dot{c}_{fresh}$)

- a term connecting spark ignition combustion to spontaneous one (b)

"b" is added to equation source term because burnt mixture (having b = 0) has already reacted, and it can not give any further heat release contribution. Once progress variable equations have been solved, the "Update composition" script computes species formed by combustion from obtained cell pressure, temperature, c or c_{fresh} and mixture fraction, and chemical products of combustion process can eventually be obtained.

Engine presentation

Engine analysed is a natural gas powered one for heavy duty applications. To reduce computational time required, just the power cycle (compression, combustion and expansion) is simulated. Figure 3 compares the whole CFD domain at the starting point of the simulation (at the intake valve closing, IVC) with respect to the top dead centre piston position. To further reduce computational time, axial symmetry has been imposed: in figure 4 a name is attributed for every mesh boundary but the left one as it is the axis of symmetry, and figure 5 shows how the whole region modeled is a small 2° arc of the whole cylinder.

Figure 3: CFD domain at intake valve closing (leftwards) and at top dead centre (rightwards)

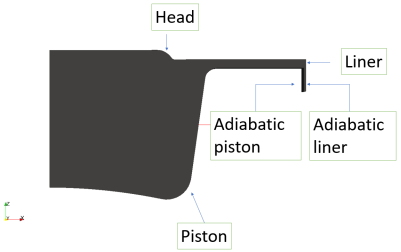

Figure 4: Cylinder walls names

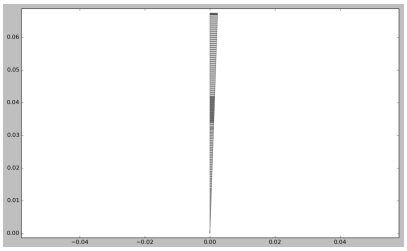

Figure 5: OpenFOAM mesh top view

Displacement of the modeled cylinder is 2.14 liters. Squish region designed is important to increase turbulence presence inside the combustion chamber, and then to have a flame propagating quickly in the whole domain considered. Walls closing the crevice regions are called "Adiabatic Piston" and "Adiabatic Liner" because that region is so small that considering no heat transfer is influencing flame propagation simulation results. In any

case, this part of the whole domain is going to be analysed when dealing with knock and spontaneous ignition, as it is located very far from the spark light and the assumption made can influence simulations results. The most important geometrical and turbulence parameters are listed in table 1. As just one power cycle is simulated, turbulence presence in the engine must be initialized a priori at the beginning of the simulation, also because no gas exchange across inlet or outlet valve is considered. As already described, intake valve closing coincides with the beginning of the simulation while the exhaust valve opening with the ending of it, hence a period of 299° is computed with respect to the 720° of the whole Otto cycle. Compression ratio adopted is 11.7,which leads to have no important knock problems when natural gas is used.

stroke	0.135 m	swirl/RPM	1.5
bore	0.15 m	swirlAxis	(0 0 1)
cRodLength	0.230	swirlProfile	10^{-5}
IVC	-175°	uprime/Up	0.7
EVO	124°	lint/Bore	0.017

Table 1: Engine main geometrical parameters

This engine design has been chosen because a map of experimental data is available: as illustrated in figure 6, some working points have been provided in "Torque-Engine speed" map and their availability is essential to tune CFD solver parameters.

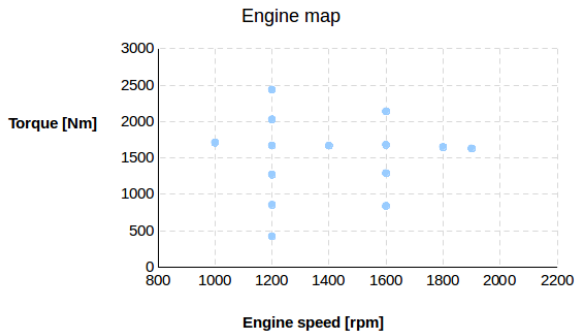

Figure 6: Engine map of experimental working points available

As illustrated in table 2, for every working point drawn in figure 6 spark timing, cylinder pressure, cylinder temperature and all wall temperatures are known at the intake valve closing condition. In addition, for all of them not just the final gross indicated work or heat release value are available, but even experimental mixture pressure, heat released and heat transfer ongoing along the whole cycle are all plotted with respect to crank angle degrees.

	1000-1710	1200-1670
Spark time	-9.75°	-11°
IVC pressure	1.72 bar	1.72 bar
IVC temperature	358 K	362 K
T_{wall} head	508 K	510 K
T_{wall} liner	420 K	420 K
T_{wall} piston	570 K	563 K

Table 2: Initial available pressure, temperatures and spark timing for every experimental working point represented in CFD map

Working points name is derived by the combination of engine speed and torque: for instance, 1000-1710 means 1710 Nm of torque at 1000 rpm. A spark ignition solver validation needs to be performed, in order to verify that it is able to reproduce correctly flame propagation combustion, both in terms of flame velocity and heat release. Spark plug strength is kept constant (value of 3), while its energy release duration is kept fixed at 1.25 ms, but changing in terms of engine time. To control spark ignition combustion flame velocity, Ξ_{coeff} equilibrium coefficient has been modified.

$$\Xi = 1 + \Xi_{coeff}\sqrt{\frac{u'}{S_u}}R_\eta \tag{9}$$

The higher Ξ_{coeff}, the higher flame velocity is going to be. By the expression above, it is possible to appreciate also turbulence influence in increasing flame combustion velocity. These data are hence essential to validate the solver: for every Ξ_{coeff} value in the range 0.4-0.7, the obtained pressure curve has been compared with the provided experimental one, in order to chose the coefficient value able to provide a good representation of the heat released by the flame itself.

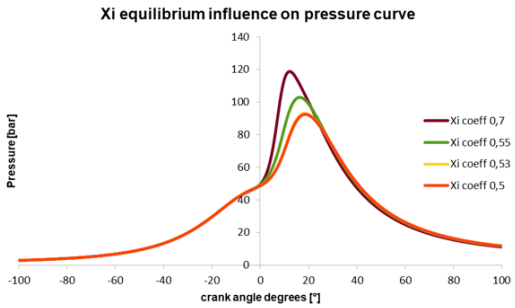

Figure 7: Xi equilibrium sweep

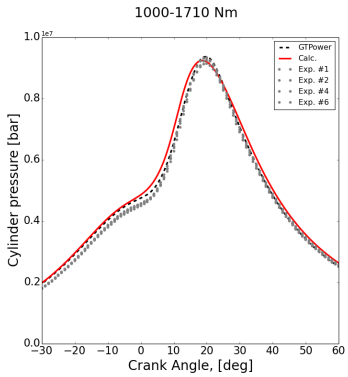

Figure 8: Experimental and Computed data comparison: cylinder pressure curve

This Ξ_{coeff} analysis has been performed in 1000-1710 working point, as it presents the lowest engine speed available, hence the turbulence influence is not so relevant (as the ratio of its intensity and engine rotational speeds is almost constant along the whole map). The Ξ_{coeff} value finally chosen is 0.5 as it is associated the most realistic pressure curve representation as illustrated in figure 8, and this obtained value has been kept constant during this work for the whole engine map. Simulation parameters are the one illustrated in the first column of table 2, and as a consequence spark timing is imposed at -9.75° with respect to top dead centre. Represented ignition delay is slightly underestimated, as the calculated curve drawn in red in figure 9 detaches a little bit too early from the dotted experimental ones, but this difference is not so important as curve trends are very similar. The only appreciable difference concerns wall heat transfer curve illustrated in figure 10: up to the minimum value, curves are almost coincident and heat losses representation can be considered realistic; but then the two curves clearly detaches leading to a huge underestimation of the computed wall heat transfer term.

Very similar results are obtained even if the other working point of the engine map are considered. Computed curves trends remain consisted with the available experimental ones, just sometimes an underestimation of the ignition delay is present but it is adjustable regulating spark timing value. As anticipated, spark plug quantity of energy released has been kept fixed.

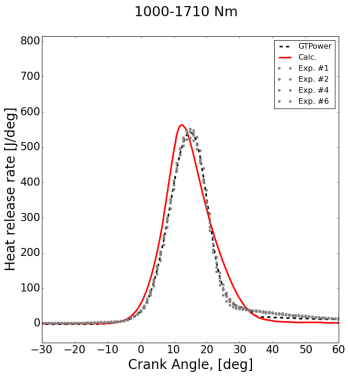

Figure 9: Experimental and Computed data comparison: rate of heat release curve

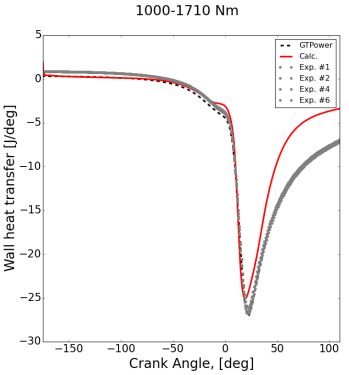

Figure 10: Experimental and Computed data comparison: wall heat transfer curve

For this validation of the flame propagation section of the solver, a natural gas entirely composed by methane has been used as a fuel, leading to no knock issues and hence no heat released by compression ignition.
Spark advance actually influences spark ignition engine performances in a considerable way, and this working points as they are not optimized can not be taken as a reference to develop a spark assisted compression ignition combustion mode. Therefore, some spark-advance sweeps have been performed in order to find the ones maximizing gross indicated work value.

Spark Ignition Engine Optimization

Anticipating the spark timing, combustion starts earlier and hence the engine can better exploit heat released by the mixture to increase maximum cylinder pressure value; but if ignition is too anticipated, both compression and heat transfer losses increase, and as a consequence thermal efficiency of the engine gets worse.

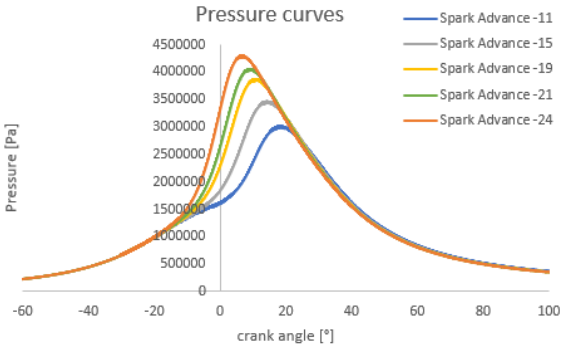

Figure 11: Spark timing sweep: pressure curves

As illustrated in figure 11, always higher maximum values are reached when ignition is advanced. Every pressure increase before top dead centre (in correspondence of 0°) is enhancing compression losses, hence the piston spends a higher quantity of energy; but, it leads to a higher underlying area during the expansion stroke, as clearly visible in the figure above.

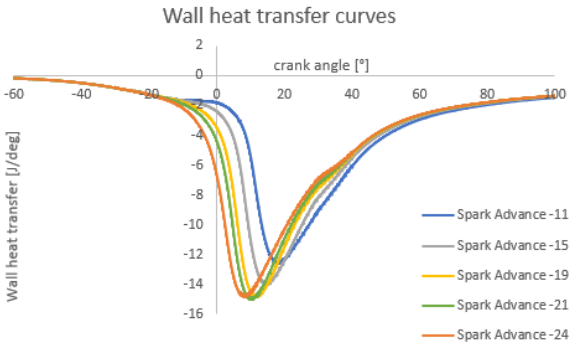

Figure 12: Spark timing sweep: wall heat transfer

Also heat losses are influenced by start of ignition: the more it is anticipated, the more time available for the mixture to loose a part of the heat previously released. This effect influences especially the second part of expansion stroke, when combustion can be considered fully completed and hence no further heat released is present. Even if results are plotted in pressure-volume plane, it is possible to appreciate how the cycle gets more ideal when ignition is anticipated. As illustrated in figure 13, combustion always gets similar to a constant volume one, increasing cycle underlying area.

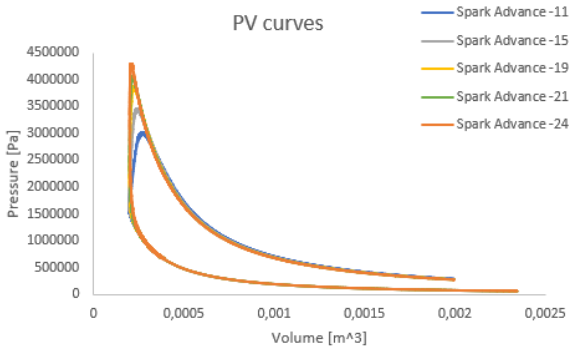

Figure 13: Spark timing sweep: pressure-volume plane

In 1000 rpm full load case, the spark timing which optimizes useful work done by the thermal machine is -19°. In order to compare even different load conditions, engine efficiency has been defined.

$$\eta = \frac{GIW}{cumRoHR} \tag{10}$$

As in equation 10, thermal efficiency is computed

through the ratio of gross indicated work obtained by the power cycle and the whole energy released by the fuel. In spark ignition engines, the load is modified increasing or decreasing both air and fuel mass injected in the cylinder. Figure 14 has been obtained keeping constant the engine speed, but varying the load: all conditions have similar temperature maximum values, but the higher thermal inertia present in high load working point leads to a lower temperature reduction, hence gross indicated work obtained at the end of expansion stroke increases. This behavior explains why turbochargers are so important for internal combustion engines, as higher initial pressures lead at the same time to have more useful work and lower losses.

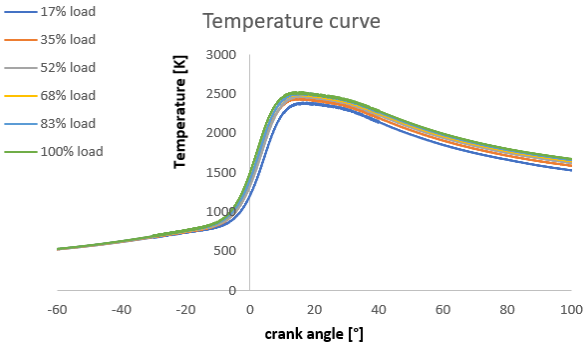

Figure 14: Temperature curves at different load

Therefore, an efficiency map considering all points available of the whole engine map has been obtained. Spark advance optimization as illustrated so far has been performed in all conditions available, and this values are taken as a reference once spark assisted compression ignition engine has been developed. As previously illustrated, at constant rotational speed, high loads working points present a higher efficiency with respect to low-load ones: if 1200 rpm working points efficiencies in figure 15 are observed, there is a difference of almost 3% between lowest load (17%) to the full load conditions. Then, due to the presence of higher turbulence intensity and lower heat transfer, efficiency values slightly improves when engine becomes faster.

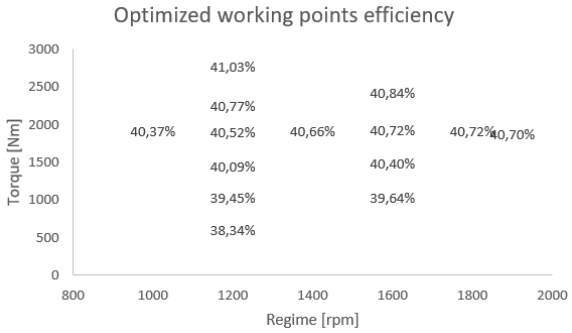

Figure 15: Engine efficiency map

These are hence the reference values to overcome of the spark ignition engine analysed. From now on, a knock analysis has been performed, in order to verify if some autoignition issues are present and if the solver behaves correctly. Then, a spark assisted compression ignition has been developed, to understand if it can lead to appreciable advantages to engine performances.

Natural gas knock analysis

Dealing with natural gas autoignition is always complicated because this kind of fuel octane number is not commercially defined, but it can vary region by region. Octane number is an autoignition indicator, assuming the value of 100 if the fuel behaves as isooctane, higher if it is more knock resistant. Natural gas usually has an octane number between 120-130, and it can change between one composition and another. In this section, a first focus has been pointed on the fuel, then on how the solver behaves whenever its hydrocarbons composition changes.
Natural gas is mainly composed by methane in all over the world. CH_4 is the lightest hydrocarbon available, a very stable molecule with an octane number of 130, but the presence of heavier hydrocarbons molecules considerably influences fuel behavior in combustion reactions. Therefore, in table 3 most important fuel heat releasing molecules are illustrated, with respective octane number (ON).

HC	Ch. formula	LHV[MJ/kg]	ON
methane	CH_4	50,0	130
ethane	C_2H_6	47,622	108
propane	C_3H_8	46,35	103
butane	C_4H_{10}	45,75	91

Table 3: Natural gas main hydrocarbons

To find hydrocarbon molecules heavier than butane is very uncommon in natural gas. If values of table 3 are observed, LHV of the molecules do not change so much, hence when passing from a natural gas composition to another (without considering possible nitrogen and/or carbon dioxide presence) heat released are almost coincident. This is not valid for octane number column, as a huge presence of propane or butane can lead to knock. Therefore, a natural gas composition investigation has been performed comparing different sources: they all agreed that in Italy (named as "Nazionale" in figure 16) there is a huge methane prevalence, while in the rest of Europe fuel is quite heavier.

Composizione media del Gas Naturale trasportato in Italia (2008) da SNAM Rete Gas

% mol	Russia	Nord Europa	Algeria	Libia	GNL	Nazionale
Metano	97,532	90,520	88,182	85,511	90,369	98,843
Etano	1,032	4,514	6,993	6,762	7,701	0,415
Propano	0,330	0,916	1,291	1,956	0,973	0,112
Butano+superiori	0,128	0,374	0,418	0,956	0,184	0,041
N2	0,836	2,390	2,151	3,409	0,773	0,508
CO2	0,142	1,286	0,965	1,406	0,000	0,081
PCS (kJ/Sm3)	38005	38543	39689	40,386	40386	37779
WI (kJ/Sm3)	50346	49186	50160	51795	51795	50418

(Fonte: Snam Rete Gas V. Cannizzo Forum Gas Milano 2009).

Figure 16: SNAM provided natural gas composition in more regions

As illustrated in figure above, nitrogen and carbon dioxide are the most common inerts present in natural gas. Since they are not involved in any combustion reaction, their presence increases octane number of the whole fuel, as chemical activity of oxygen is reduced. At the same time, lower heating value of the fuel decreases as they can not take part to any combustion reaction. Values displayed in figure 16 are computed in mole percentages, hence when passing to mass ones heavier hydrocarbons values becomes higher. In the end, even after converting these numbers, almost all natural gases commercially available have a methane mass percentage higher than 85%, with ethane as the second main hydrocarbon. Very low mass percentages of propane or butane are enough to let the engine knock, as just the 4% of them can start autoignition chain reactions. As already described, two different kinds of combustion coexist in the solver. Flame propagation velocity has been validated determining the most suitable Ξ_{coeff}, while an external experimental study is needed to perform natural gas knock validation. This subsection is fully dedicated to comparison between solver results and a paper published in 2012 by Jiri Vavra, Michal Takats, Vojtech Klir and Marcel Skarohlid of the Czech Technical University, named ["Influence of Natural Gas Composition on Turbocharged Stoichiometric SI Engine Performance"].
In this study, knock tendency of a compressed natural gas engine has been investigated including some additives to a reference fuel composition. Engine has hence been tested with a multiplicity of different fuels, in order to detect if knock is occurring or not. If the solver can reproduce results comparable with experimental values, validation can be considered completed and the solver able to be used for design purposes; but it is impossible to get coincident results, as some important parameters such as experimental study combustion chamber design are not reported. In any case, if a result consistency is detected, validation can be considered completed. In the CFD solver, knock occurs whenever the normalized progress variable c_{fresh} reaches the value of unity, starting the so-called compression ignition combustion; in the experimental study, an AKR sensor has been used, returning a voltage output proportional to knock intensity. If the knock recognizing sensor signal is higher than 2 V, autoignition is considered heavy, otherwise it is light. Exploiting pressure curves available in the published paper, conversion value between the sensor output and knock associated pressure rise is 2.16 knocking bar/V.

CH_4	96.73%
C_2H_6	0.82%
C_3H_8	0.44%
C_4H_{10}	0.38%
N_2	1.44%
CO_2	0.19%

Table 4: Reference natural gas composition to be tested

In table 4, reference fuel composition taken from Czech grid has been described. Some ethane, propane or butane has been added to the fuel, obtaining heavier natural gases to let the engine knock. Another important thing to be highlighted is that the engine tested in the experimental publication is very similar to the CNG-heavy duty one. As already anticipated, its combustion chamber design is unknown, but as suggested by table 5 both geometrical parameters and intake maximum pressures are very similar.

	paper engine	CNG-heavy duty
CR	12:1	11.7:1
Max pressure	2.4 bar	2.44 bar
Bore	102 mm	135 mm
Stroke	120 mm	150 mm
IVC	-125°	-175°
EVO	123°	124°
ϕ	1	1

Table 5: Comparison between paper engine and CNG-heavy duty one

By a solver point of view, a different Cantera table must be generated for every kind of fuel analysed.

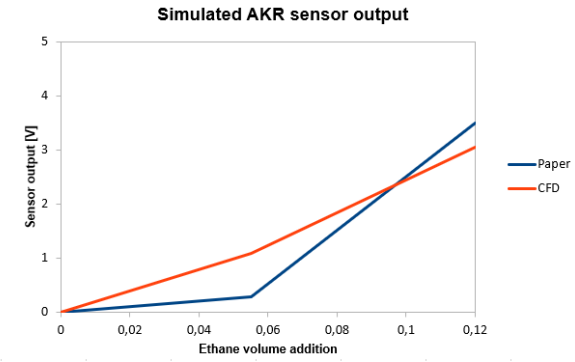

Figure 17: Simulated AKR output sensor in ethane addition

As it is possible to see in figure 17, there are some differences between the computed knock intensity and the experimental one. In any case, a more realistic representation would be too pretentious, also because combustion chambers compared have different sizes. What is important to remark is that results consistency is maintained along different experiments shown in figures 18 and 19, which can lead to an appreciable consideration regarding natural gas spontaneous ignition representation.

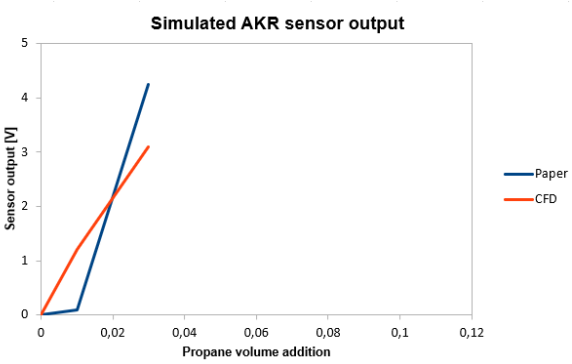

Figure 18: Simulated AKR output sensor in propane addition

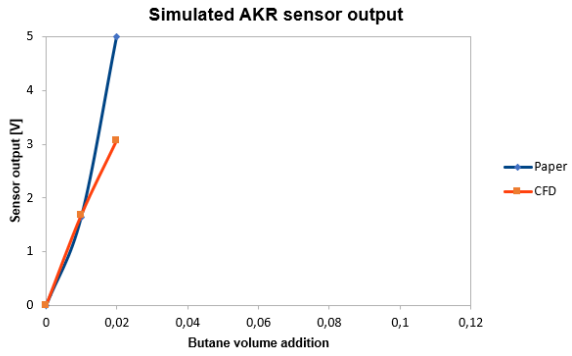

Figure 19: Simulated AKR output sensor in butane addition

Once the solver can be considered reliable, focus is pointed on how knock is reproduced in the CFD domain. As already specified, autoignition starts whenever c_{fresh} normalized reaches the value of unity. As predicted by theory and displayed in figure 20, spontaneous ignition starts in most external region, where squish area is located. It requires time to start, hence a slow flame or a big cylinder bore enhance its probability. In the figure below, leftwards the flame front is displayed, while rightwards just compression ignition associated progress variable is represented in the CFD domain. In any case, compression ratio adopted

in CNG-heavy duty engine is too low to have an appreciable autoignition, hence a new natural gas composition has been edited in order to let the engine knock.

	SNAM	heavy Natural Gas
Methane	81.88 %	84 %
Ethane	7.65%	8%
Propane	2.28%	6%
Butane	1.23%	2%
Nitrogen	3.77%	
Carbon Dioxide	3.19%	

Table 6: Natural gas composition in mass percentages

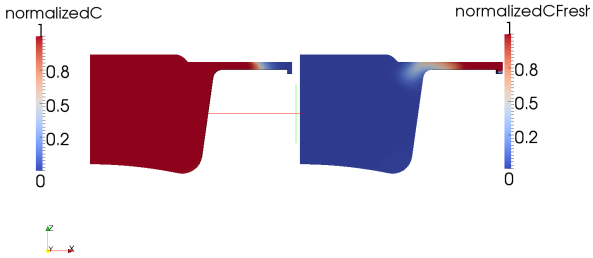

Figure 20: Engine flame front and spontaneous ignition visualization

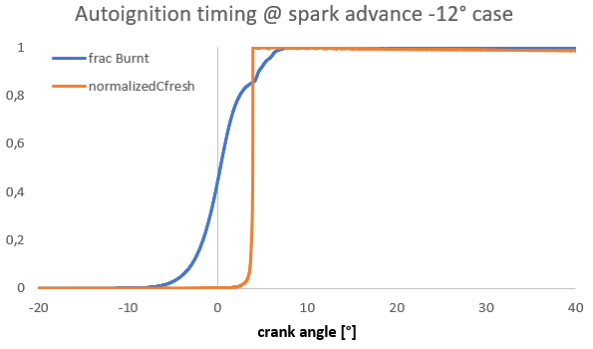

Figure 21: Autoignition progress variable increase

In table 6, the edited fuel named as "heavy Natural Gas" is reported. This kind of fuel composition is very heavy and hence unlike to be found in ordinary fuel station, but it guarantees the knock presence once fed in CNG-heavy duty engine. Close to it, SNAM North Europe derived natural gas composition is reported in mass percentages, as it is the one used from the next section on to design spark assisted compression ignition engine. Charts plotted in figure 21 shows how spontaneous ignition progress variable increases in a really fast way. In the illustrated case, it appears after the 80% of the whole amount of fuel has already ignited by flame propagation. As soon as the first mixture particle auto-ignites, it releases an appreciable amount of heat needed to start a sort of compression ignition flame, which is oriented from the most external part of the cylinder to the most internal one. In any case, it can not be considered a proper flame, as usually it is very violent and associated to very severe and unwanted pressure waves; but in terms of compression ignition progress variable transport, it behaves similarly to an incredibly fast flame propagation combustion.

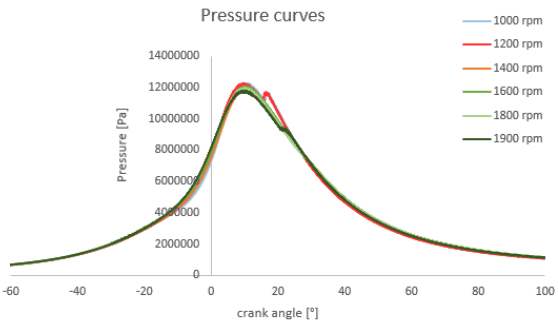

Figure 22: Pressure curves for heavy Natural Gas powered engine

As shown in figure 22, a rotational speed sweep has been performed to verify knock presence and intensity for any available constant torque condition. Compression ignition can in fact be easily detected by the presence of a very vertical pressure increase when it takes place. As displayed by the figure above, this increase is heavier at low rotational speeds, but final part of combustion results faster and pressure curve underlying area gets wider. This explains the potentiality of spontaneous combustion in homogeneous charge condition, as it results faster and hence more ideal. Every simulation has

been carried in optimized spark timing condition, as previously illustrated.

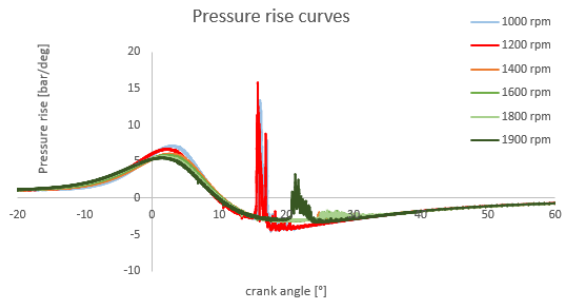

Figure 23: Pressure rise curves for heavy Natural Gas powered engine

In figure 23, pressure rise of obtained curves is plotted. Even if compression ignition contribution to cylinder pressure is not enormous, maximum rise displayed in this curve is very close to the assumed mechanical limit of the engine. In addition, after spontaneous ignition occurred some values oscillations are present: they are due to the mechanical wave originated by this huge amount of heat released, but time step and turbulence model set in the solver can not lead to a realistic representation of these kinds of waves.

Development of a spark assisted compression ignition engine

In previous section CNG-heavy duty engine could knock only if powered with very heavy natural gas, unlikely to be found in ordinary fuel stations. To develop a SACI (spark assisted compression ignition) combustion, spontaneous ignition must be reliable and under control, not depending on kind of natural gas used. Therefore, compression ratio has been increased to have higher pressures and temperatures and then enhance fresh air-fuel mixture autoignition. This leads to a redesign of combustion chamber, performed in such a way to increase the compression ratio adopted but to not introduce significant changes on piston shape.

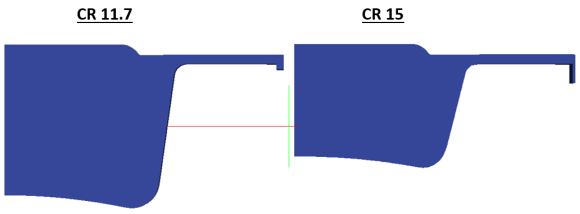

Figure 24: Combustion chamber shapes at top dead centre

As it is possible to see in figure 24 where original design and the new one are compared, volume at top dead centre of increased compression ratio chamber is far way lower. Parameters such as bore and stroke are not changed, so this kind of modification practically implies just a substitution of the original piston with a new one.

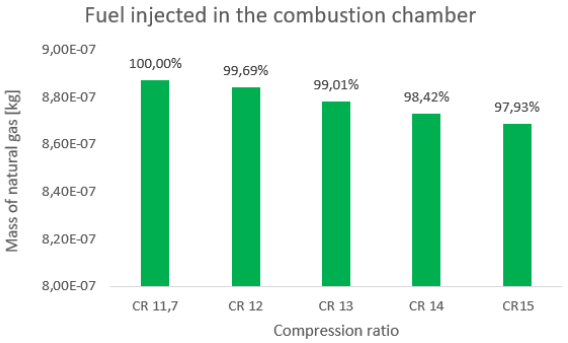

Figure 25: Mass of fuel injected in different compression ratio engines

As it is evident by figure 25, considering the same working points (characterized by initial cylinder pressure and temperatures values) a lower mass of fuel is injected inside the cylinder. This leads to a first advantage in terms of efficiency: as shown in figure above, for the same initial pressure and temperature values, in the CR 15 case fuel amount is more than 2% lower with respect to the reference one at CR 11.7. In addition, since a better thermal efficiency is predicted as explained by the theory in section 1, even gross indicated work should increase, leading to another efficiency benefit. Also knock must be taken into account: in a spark as-

sisted engine, it needs to be controlled to be exploited for a more ideal constant volume combustion. At this purpose, two different solvers are used in this section:

- Xi solver: including b equation

- SACI solver: including b and c_{fresh} equations

As briefly described, the "Xi" solver can not consider autoignition, and as a consequence it is possible to simulate very extreme compression ratio engines without any knock presence. "SACI" solver instead includes both flame propagation combustion and chemical reaction delay time, computing also heat released by a possible mixture autoignition. A comparison between these two solver results is very important to isolate combustion mode influence from all the other parameters that affect the power cycle, and to have more clear advantages and disadvantages concerning just spontaneous ignition. As already proved, autoignition can be very rough and violent, stressing in a dangerous way mechanical engine resistance. Due to the almost instantaneous heat release, it is possible to reach very high cylinder pressure values and, if bad controlled, it can turn into heavy knock. For this reason, not all the working points in the engine map can work using a SACI combustion mode, but just the ones at half load or lower. In figure 26 displayed below engine map is revisited, with SACI combustion target points drawn in green, while entirely flame propagation combustion target points in red.

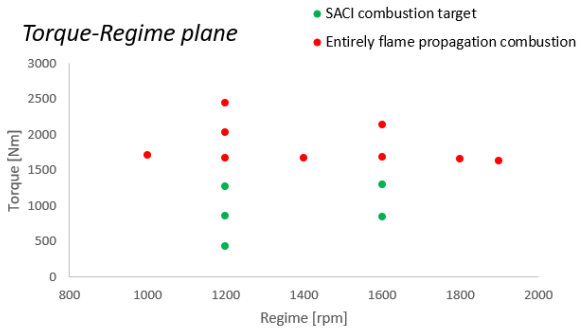

Figure 26: Revisited engine map, showing SACI and flame propagation points

To perform the illustrated solvers results comparison, 1200 rpm - half load working point has been considered. Natural gas composition used is the SNAM source derived North Europe one illustrated in table 6, and compression ratio adopted is 15, which is a very high value for a spark ignition engine.

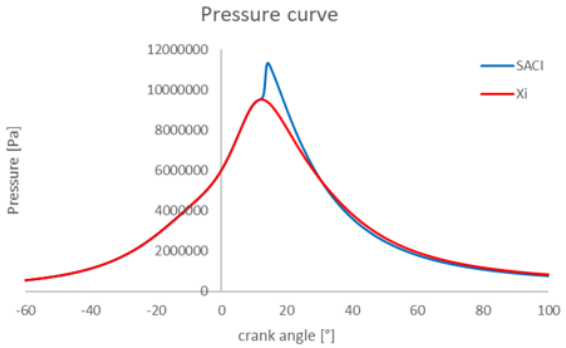

Figure 27: Pressure curves obtained by both solvers in the same initial conditions

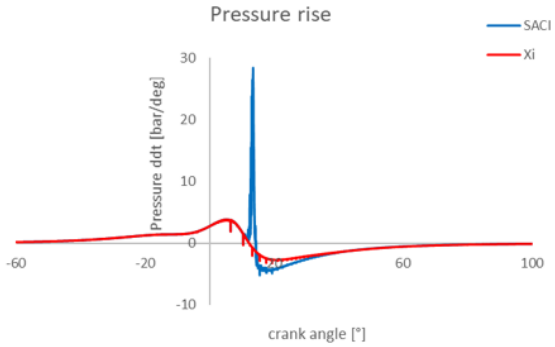

Figure 28: Pressure rise curves obtained by both solvers in the same initial conditions

As illustrated by figure 27, spontaneous ignition occurs in correspondence of maximum pressure value, evidently increasing SACI solver curve underlying area. A spark timing of -16° has been imposed to both the cases, as well as SNAM North Europe derived natural gas composition (the same that could not autoignite in previous section) has been used. Because of spontaneous ignition, pressure maximum value increases considerably, over than 20% in relative terms. Especially regarding cumulative heat release curve of figure 29, one

can appreciate how fast compression ignition combustion is in homogeneous mixture conditions: in the case where it is included in the solver, combustion ends between 13-14° crank angle, almost 20° before entirely flame propagation combustion is completed. This of course leads to a very severe and dangerous pressure rise, that overcomes enormously the already high assumed limit. As shown in figure 28, pressure rise is close to 30 bar/deg, a very high value, especially for a half load condition.

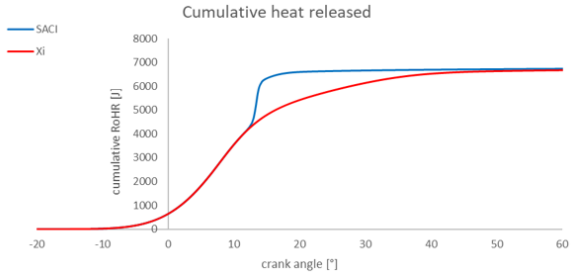

Figure 29: Cumulative heat release curves obtained by both solvers in the same initial conditions

	η	GIW	cum Heat losses
SACI	40.78%	2759 J	-1359 J/deg
Xi	41.89%	2827 J	-927 J/deg

Table 7: SACI and Xi solvers comparison

If cumulative gross indicated works are compared, result obtained seems in contradiction with pressure curves previously illustrated. As shown in table 7, both gross indicated work and hence efficiency values are lower whenever compression ignition is implemented in the solver. To have a better knowledge of work during the cycle, instantaneous gross indicated work is computed as illustrated in equation below:

$$GIW_{Inst} = \frac{p \cdot \Delta V}{\Delta\theta} = \frac{\frac{p_i + p_{i+1}}{2} \cdot (V_{i+1} - V_i)}{\theta_{i+1} - \theta_i} \quad (11)$$

Where in the equation 11 "i" stands for time step considered, "p" for cylinder pressures, "V" for combustion chamber volume and, in the end, "$\Delta\theta$ for the time step used computed in crank angles, in the order of magnitude of thousands of crank angle degrees.

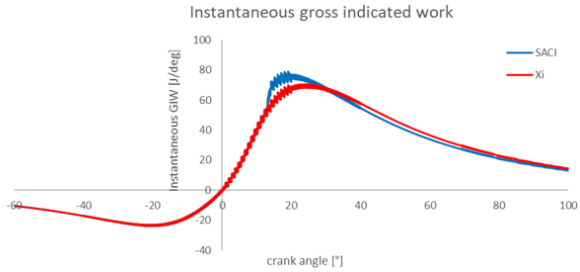

Figure 30: Instantaneous gross indicated work curves obtained by both solvers in the same initial conditions

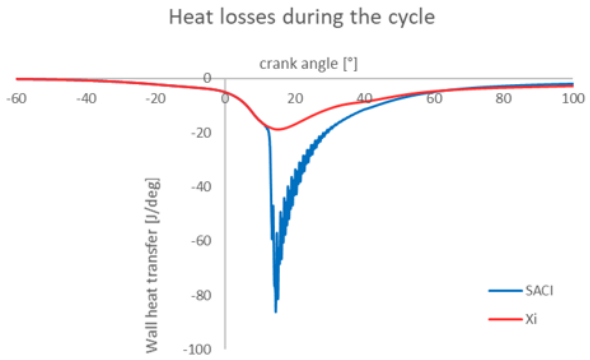

Figure 31: Wall heat transfer curves obtained by both solvers in the same initial conditions

Observing figure 30, the two curves are coincident up to spontaneous combustion presence, which increases blue curve pressure values hence instantaneous work made by burnt gases. Even if the detach is clear, in less than 20° the curves intertwine, and expansion computed by "Xi" solver is clearly more efficient with respect to the one computed by "SACI" once both combustions are completed. Wall heat transfer minimum value in knock presence is more than four times lower than the one computed by "Xi" solver reported in red. Effects on temperature curves are enormous since immediately after compression ignition weighted average maximum values are higher of 300 - 400 K, but then burnt mixture cools down in a very fast way and blue curve negative slopes after compression ignition are considerable. Burnt mixture has hence less energy to be exploited for almost all the second part of expansion stroke, and cumulative gross indicated work gets lower at the end of the cycle.

This leads to a sort of paradox, because with spark assisted compression ignition a more ideal combustion mode has been reached, but losses are so important to considerably reduce power cycle work and efficiency.

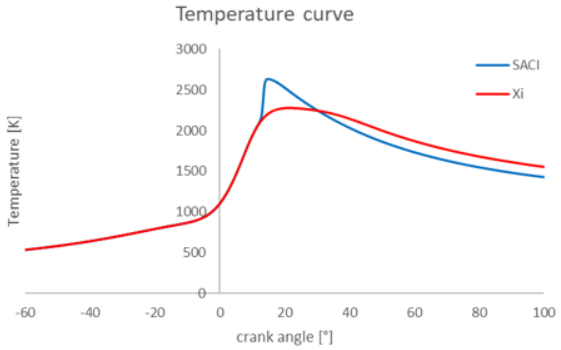

Figure 32: Temperature curves obtained by both solvers in the same initial conditions

Knock is defined by theory as an abnormal combustion in a spark ignition Otto cycle engine that can be recognized by the presence of metallic noise coming from the engine. It origins pressure waves which, propagating in the combustion chamber and rebounding in correspondence of cylinder walls, reduce power cycle efficiency and hence gross indicated work, even if the whole combustion process needs less time to be completed. In this thesis work, knock caused performance loss is associated to a wall heat transfer increase due to turbulence generated by the wave itself.

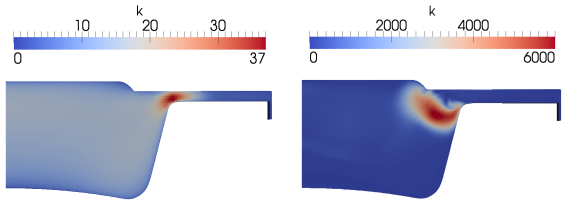

Figure 33: Turbulence intensity comparison between before (left) and after (right) autoignition

Therefore, in figure 33 it is possible to see two turbulent kinetic energy time step values of the same case: leftwards, during flame propagation but before autoignition appearance; rightwards once spontaneous ignition is almost completed and huge heat has been released. As evident, maximum κ values differs of more than two orders of magnitude. In a entire spark ignition context, turbulent kinetic energy reaches its maximum values very close to squish area, which is designed to increase fluid turbulence and hence flame velocity; after autoignition occurs, κ reaches its maximum values as soon as the fluid is exiting from the squish area to go towards inner parts of the combustion chamber, as soon as there is more space for the pressure wave to propagate.

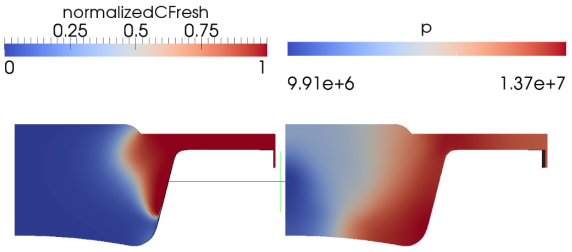

Figure 34: Pressure gradient after wave has propagated inside the combustion chamber, 11 deg after TDC

This behavior is strongly connected to pressure waves presence, which move from the most external cylinder region to the inner of the combustion chamber, to then rebound in correspondence of cylinder walls. This kind of behavior is actually typical of all knocks met so far, and it provides a further explanation on performance decrease encountered. Some crank angle degrees after spontaneous ignition is completed, pressure gradient inside the combustion chamber becomes maximum, with pressure differences of over than 30% in most severe knock condition. All of it is contributing into increasing kinetic energy of the working fluid, and as a consequence heat transfer coefficient between the fluid and the wall, explaining also why heat transfer curve and turbulent kinetic energy ones have such a similar behavior.
As a consequence, to reduce the pressure wave intensity is fundamental for a good exploitation of spontaneous ignition combustion; two different strategies are hence investigated: piston shape changes and leaner air fuel ratio. The first one can be explained by these last considerations, showing

that pressure waves are enhance by squish region; the second aims to have both a far way less violent compression ignition and to have more thermal inertia of gases inside the cylinder, in order to reduce heat losses.

Piston shape analysis to exploit CI combustion

It has been demonstrated how squish region is important for flame properties but also detrimental for a good exploitation of compression ignition. Heat released from homogeneous charge autoignition is far way faster than the one coming from flame propagation; hence combustion chamber has been redesigned in the external region with the aim of taking benefits of this combustion mode, keeping the same compression ratio. Most important geometrical parameters such as stroke, bore or cylinder head shape have not been changed to not impose huge modifications to the engine, but just piston shape is investigated.

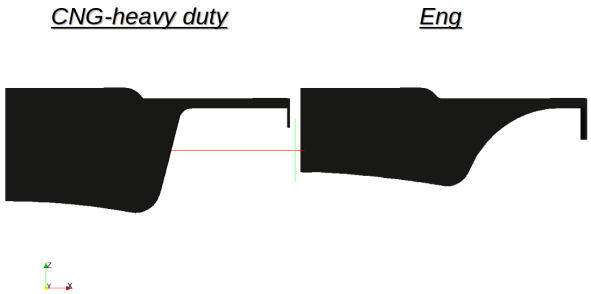

Figure 35: Piston geometry comparison at top dead centre

In figure 35 geometry changes are illustrated, with both images taken in correspondence of top dead centre piston position. Some more space has been added in correspondence of squish area, in such a way to expand the pressure wave originated by compression ignition. The extension of this region forces the designer to reduce the distance between cylinder head and piston in the central part of the combustion chamber (in correspondence of the axis of symmetry), and for flame propagation this is a huge disadvantage because flame front surface will be lower and combustion is predicted slower than before. Taking in consideration these assumptions, also a third piston geometry has been simulated, called "Turb". Just this last combustion chamber design has a slightly lower compression ratio (14.8), and it has been edited to find a good exploitation of flame surface properties.

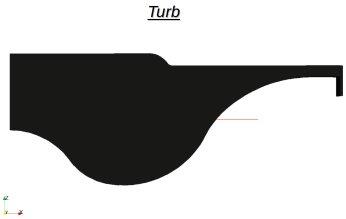

Figure 36: "Turb" piston geometry at top dead centre

In both of these two last edited geometries, importance and influence of squish area have been remarkably sacrificed to exploit homogeneous charge compression ignition, which in CNG-heavy duty geometry was too violent.

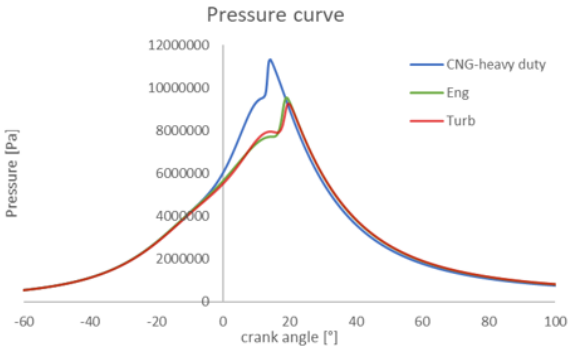

Figure 37: Pressure curves associated to different piston geometries

From figure 37 displayed above, it is evident how combustion is far way slower in "Eng" and "Turb" geometries, which have almost coincident pressure curves. Spark ignition combustion in CNG-heavy duty engine is considerably faster but pressure rises due to autoignition of the three cases are comparable. As predicted, combustion velocity is reduced because of the lower flame front surface but also to the lower turbulence intensity presence, as shown in the figure below.

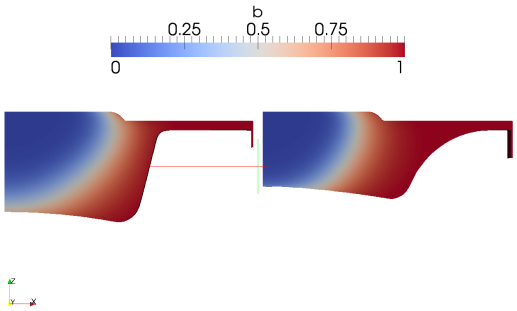

Figure 38: Flame front in CFD domain associated to different piston geometries

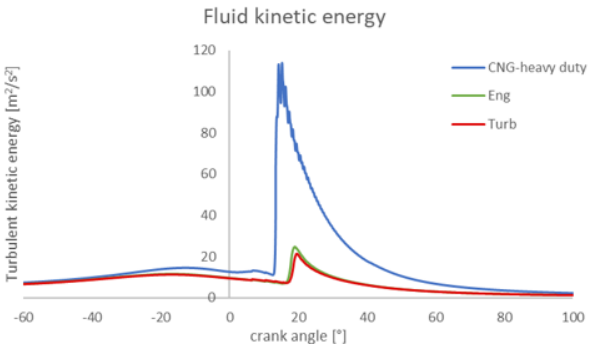

Figure 39: Turbulence intensity weighted average associated to different piston geometries

Figure 38 reported above illustrates in a good way how CNG-heavy duty geometry presents a flame front with a higher surface, leading to considerable advantages for combustion. Even if combustion development has been slowed down, power cycle efficiency values between the three different cases are comparable: in table 8, efficiency values are reported, showing how even if flame propagation is this slow both "Eng" and "Turb" geometries are more efficient with respect to the CNG-heavy duty one. Therefore, a spark advance sweep has been performed for both the geometries but, as they lead to very similar considerations, just the "Turb" one is illustrated.

	solver	η
CNG-heavy duty	SACI	40.78%
Eng	SACI	41.69%
Turb	SACI	42.01%
CNG-heavy duty	Xi	41.89%

Table 8: Efficiencies comparison of different piston geometries, with the same initial conditions and spark timing

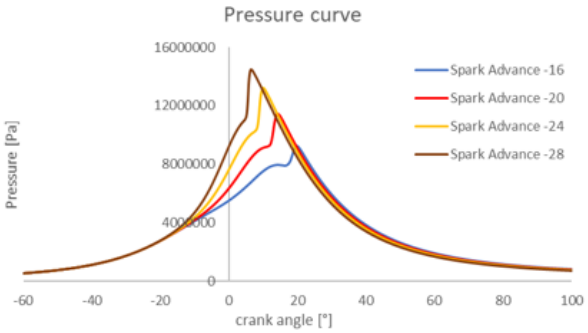

Figure 40: "Turb" pressure curves in spark timing sweep

Pressure curves behavior (shown in figure 40) is consistent with the one previously analysed. Compression ignition is occurring in every cycle, with an increasing intensity as spark timing is anticipated. Maximum efficiency is reached at -20° of spark timing, hence compression ignition in this case is not something to be absolutely avoided. In figure 41 it is shown autoignition development from its origin (11°) to its ending (14°). Changing in squish area is also important to give a shape or compression ignition development, as happens with flames. When squish area was adopted, as soon as autoignited mixture has more space, it developed in a messy way, originating pressure waves. With this geometry, c_{fresh} has a more defined shape very similar to the one of a flame coming from most external regions, hence wave generated is far way lower leading to heat losses reduction.

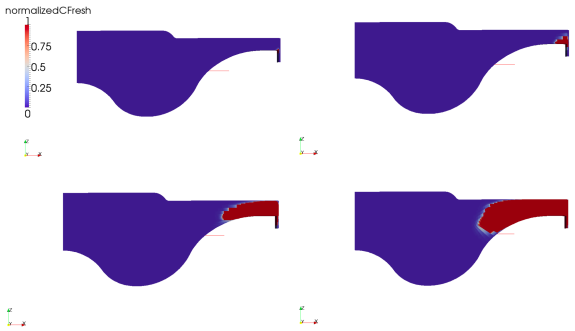

Figure 41: Compression ignition evolution between 11 deg and 14 deg in "Turb" geometry

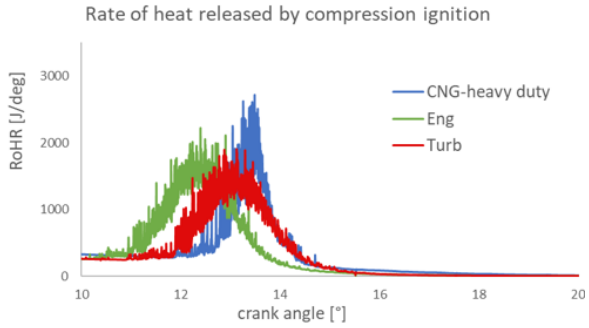

Figure 42: Rate of heat released by compression ignition comparison between different geometries

If figure 42 is observed, it is evident how different piston geometries can influence compression ignition heat release: in both the edited ones, maximum rate of heat released value is lower and, at the same time, bells associated to compression ignition are wider, meaning it is requiring more time to be completed. These effects combined lead to a softer combustion mode, and intensity of pressure waves generated is far way lower. Charts reported in figure 43 are a direct consequence of this characteristic: as lower pressure gradients are present in combustion chamber, fluid kinetic energy does not increase that much and a lower heat amount is lost. As obtained when different solver results were compared, heat losses penalize work done by burnt gases in the final part of expansion stroke, after 40 CAD. In this way, advantage of the presence of spontaneous ignition is maintained, and at the same time heat losses are reduced in such a way to not penalize work done during the expansion stroke.

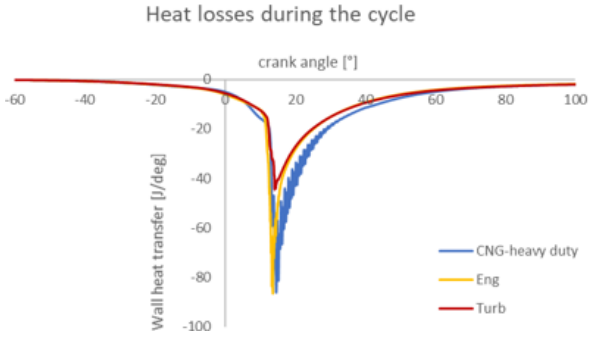

Figure 43: Wall heat transfer comparison between different geometries

With the previous CNG-heavy duty combustion chamber geometry, compression ignition was something to be avoided as it decreased useful work done by the thermal machine. In this case, as illustrated by the efficiency curve in figure 44, peak is located in correspondence of a spark advance of 20°, with more than 30% autoignited mixture mass. Therefore, the value of 41.89% obtained by the Xi solver in a fast combustion geometry has been definitely overtaken, and compression ignition can be exploited even in stoichiometric mixture charge conditions. As previously illustrated, not all the working points represented in the engine map can run with this combustion mode, because it would result with very high pressure rise values dangerous for the mechanical resistance of the engine.

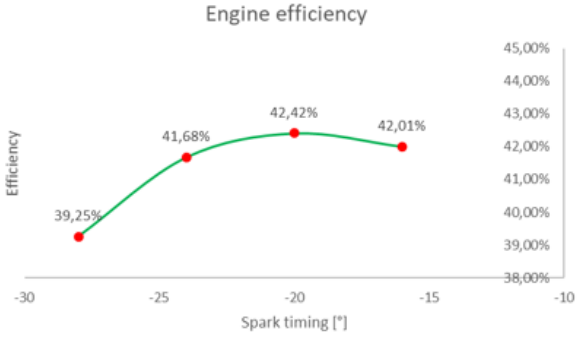

Figure 44: Efficiency curve for "Turb" piston geometry running at stoichiometric mixture

Design a combustion chamber with such a low

flame propagation velocity can lead to several problems when full load condition is simulated, as spark timing needs to be delayed to avoid autoignition and, at the same time, the flame is slow and pressure peak is far from the top dead centre. For this reasons, spark assisted compression ignition combustion in lean conditions is investigated, as it permits to easily pass from a lean partial load mixture to a stoichiometric full load one.

Lean SACI combustion

Piston geometry taken as a reference is the starting CNG-heavy duty one, as it presents the squish region that speeds up combustion. Equivalence ratio chosen for this analysis is 0.8, as it permits to have considerable air excess but, at the same time, to completely avoid flame extinguish. Reference efficiency value is always the 41.89% obtained simulating 52% load high compression ratio engine with the Xi solver. As thermal efficiency is the real target of this investigation, amount of fuel injected as been kept the same for all the illustrated cases: this leads to an IVC pressure increase to have the wanted air excess.

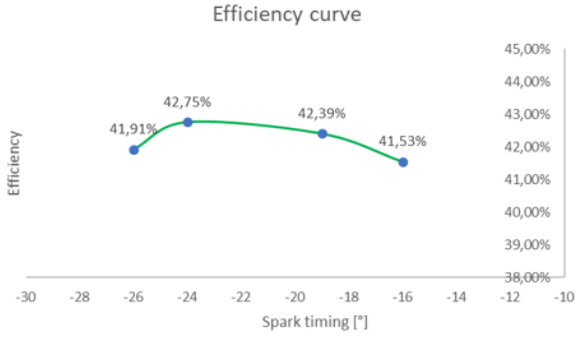

Figure 45: Efficiency curve in lean conditions

To feed the engine with lean mixture leads to appreciable efficiency improvements: maximum reached one is 42.75% taken in correspondence of -24° as spark timing. This solution can lead to implement a squish region and a compression ignition design at the same time, as stresses induced to the engine are far way lower.

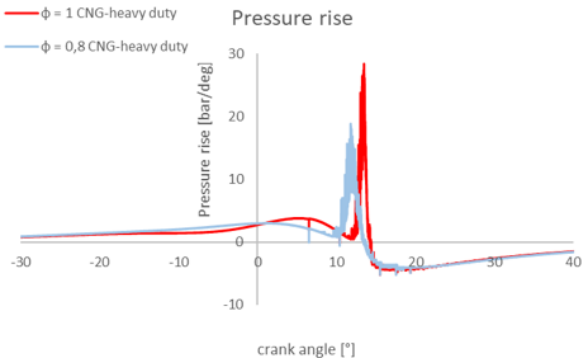

Figure 46: Pressure rise comparison between lean and stoichiometric mixtures in CNG-heavy duty piston design

In figure 46, lean spark advance optimized case is compared with the stoichiometric mixture one computed with the SACI solver. In lean case pressure rise reaches lower maximum values and it is more distributed in time: this leads to similar considerations derived by figure 42, as they can both prove a softer and well exploited compression ignition. When SACI and Xi solver results were compared, temperature has a massive decrease after compression ignition as a consequence of the huge heat transfer. In temperature curves of figure 47, no huge negative slope is present. This can be considered a result of a combination of different factors, such as the lower adiabatic flame temperature due to air excess, the lower wave intensity ad previously illustrated but also the higher thermal inertia present in the cylinder due to the increased working fluid mass.

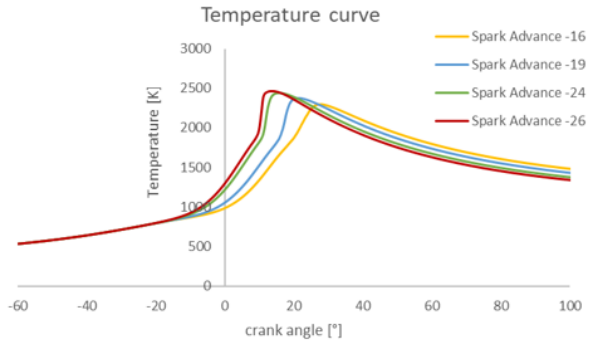

Figure 47: Temperature curves in spark timing sweep in lean conditions

Therefore, to develop a lean spark assisted compression ignition combustion can lead to the opportunity to differentiate equivalence ratio depending on the kind of combustion mode wanted for every working point. If also the two illustrated edited geometries run with some air excess, spark timing needs to be further anticipated as flame propagation is very slow. At the same time, also compression ignition is considerably slowed down, leading to an overall better combustion exploitation. As figure 48 shows, when even "Eng" and "Turb" geometries are simulated, spontaneous combustion in further slowed down. From the first simulated case to the lean "Turb" optimized one (having a spark timing of -30°) maximum rate of heat released has been more than halved, leading to an always higher control of spontaneous ignition combustion. At the same time, the presence of also this second kind of ignition leads to an appreciable combustion velocity increase even in every lean conditions. The maximum efficiency has been obtained in "Turb" geometry fed with lean air-fuel mixtures, assuming the value of 43.34%, (which is a massive increase for a half load 1200 rpm case, as the starting one in an entirely methane flame propagation combustion context was 40.09%, as show in figure 15). At the same time, what has been derived by this study is that criteria for a fast flame propagation and a well exploited spontaneous ignition combustion are somehow opposite. The overall Otto cycle becomes far way more ideal: in figure 49 the "Turb" lean case has been compared with the CNG-heavy duty one with 15 as compression ratio, evidencing how the overall cycle becomes more ideal.

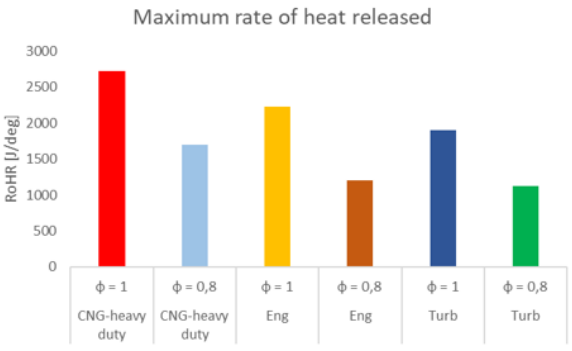

Figure 48: Maximum rate of heat released comparison between different configurations

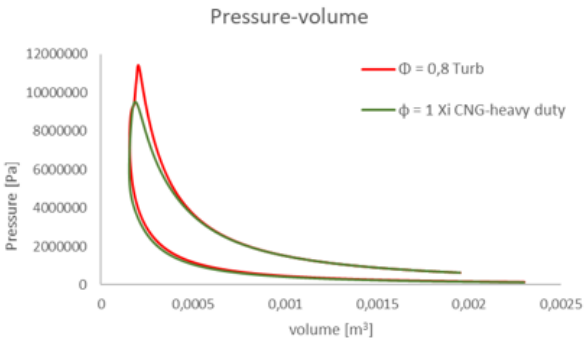

Figure 49: Pressure curves in pV plane

Even by figure above, the point of weakness of this piston configuration is the huge ignition delay: -30° as optimized spark timing at 1200 rpm is huge, and when high loads or high regimes are reached this can become an issue. For this reason, to perform the load sweep CNG-heavy duty piston shape has been chosen (with a compression ratio reduction up to 14.5), running with lean SACI combustion at half load or lower and adopting just the stoichiometric mixture flame propagation one when load is higher. All efficiency points displayed in figure 50 have been optimized with respect to spark advance. Therefore, the resulting curve is the matching of two different trends, but SACI points have always higher (or almost equal) efficiency with respect to the others. In any case, spark timing in just flame propagation working points must be considerably delayed (up to 10°), and because of that high load working points have no efficiency benefits.

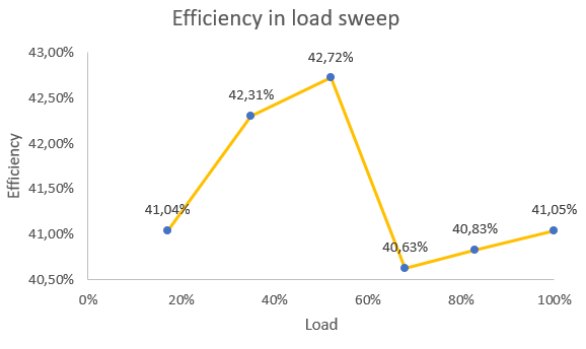

Figure 50: Efficiency-load curve of CNG-heavy duty engine at increased compression ratio

Pollutants analysis

Running the engine lean could be a problem for the three-phase catalyst since its conversion efficiency is optimized in stoichiometric air-fuel mixture condition, in which correspondence values about 95% can be reached and overtaken, consequently decreasing pollutant emissions of the whole engine. In this CFD solver after-treatment systems are not considered, hence focus is pointed on the carbon-monoxide formation during the combustion process and on the amount of unburnt hydrocarbons at the end of the power cycle.

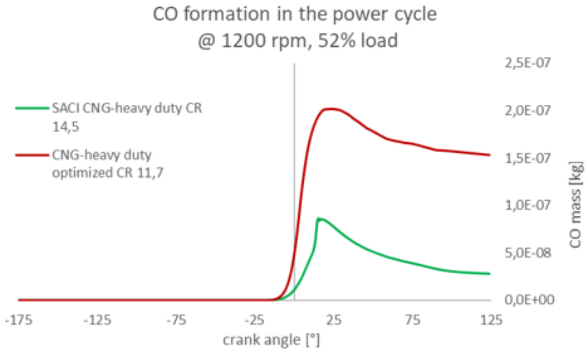

Figure 51: CO production in 1200-half load working point comparison

As evident by the figure 51, air excess enhances carbon oxidation both during and after the combustion process. Reducing the equivalence ratio from 1 to 0.8, less than the 25% of the CO is globally present at the exhaust valve opening, and this quantity is even predicted to decrease once exhaust gases cross the catalyst. Carbon oxidation proceeds with an appreciable velocity until to the end of the expansion stroke (with a slowdown at around 90° crank angle because of gases temperature reduction) and the pollutants is homogeneously distributed within the whole combustion chamber. However, not all the fuel particles can burn and then release heat: as shown by figure 52, even if at higher compression ratios a lower fuel quantity is injected in the engine (for the same initial pressure), unburnt natural gas quantity increases, probably due to a wider flame extinguish region near to cylinder walls. Always in the same figure, respective percentages representing the ratio of unburnt hydrocarbons with respect to mass of fuel injected are reported.

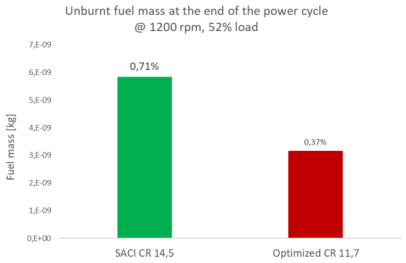

Figure 52: unburnt hydrocarbons after the whole combustion process in 1200-half load working point comparison

For what regards nitrogen-oxides emission, however the solver can not predict NOx formation. For sure, the oxygen excess is enhancing their production, but adopting a leaner mixture permits to have a lower adiabatic flame temperature hence decrease NOx production. Figure 53 reported above compares cell by cell temperatures reached in a SACI at high compression ratio with the ones of an entirely flame propagation combustion. Temperature weighted average values are higher when spontaneous combustion takes place, but this increase is given by the presence of two different combustion modes, which speed up fuel oxidation reactions. Since cell temperature maximum values in lean conditions are almost 200 K lower with respect to the stoichiometric case, these effects combined should limit the overall NOx production during the power cycle.

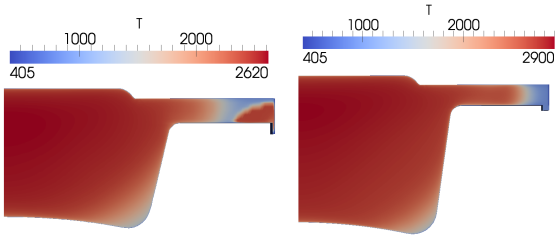

Figure 53: Cell temperatures in 1200-half load working point comparison

As already written, these calculations were performed ignoring the presence of any after-treatment system at the turbine outlet. In any case, three-phase catalyst conversion efficiency is function of

NOx, CO and hydrocarbons inlet mass, and this can be an interesting study case for future works.

Conclusions

In conclusion, spark assisted compression ignition can take to several efficiency benefits, but knock needs to be avoided. To do so, spontaneous ignition flame needs to be slowed down, and this can be done in two different ways: redesign the combustion chamber and/or using a lean air-fuel ratio. Adopting both the solutions can increase thermal efficiency considerably, passing from the 40.09% of entirely flame propagation CR 11.7 engine to the 43.34% obtained by a CR 14.8 edited on purpose geometry. The real issue of this solution is that design criteria of a fast flame propagation and ones of a well-exploited compression ignition combustion are somehow opposite, as the second starts in most external part of the cylinder where squish region in commercial spark ignition engines usually is. Therefore, another investigated strategy to exploit SACI combustion is adopting some air excess: compression ratio has been increased up to 14.5, but piston shape has not been changed. Equivalence ratio has been reduced up to 0.8, leading to a slower compression ignition flame and consequent efficiency improvements. The real weakness of lean mixture combustion is represented by three-phase catalyst conversion efficiency, which is usually optimized for stoichiometric mixture exhausts. In any case, adopting such an air excess carbon monoxide production is just the 25% of the one produced by a stoichiometric mixture in the same initial conditions, which can be an interesting object of study for possible future works.

References

[1] H. Versteeg and W. Malalasekra, *An Introduction to Computational Fluid Dynamics*, 2, Pearson India Education Services (2009)

[2] Giancarlo Ferrari, *Motori a combustione interna*, 1, Socierà editrice Esculapio (2016)

[3] D.S. Malik, *Introduction to C++ Programming*, 1, Apogeo Education (2009)

[4] Tommaso Lucchini, Angelo Onorati, Gianluca D'Errico, Alessandro Stagni and Alessio Frassoldati, *Modeling non-premixed combustion using tabulated kinetics and different flame structure assumptions*, Dipartimento di Energia, Politecnico di Milano (2017)

[5] H.G. Weller, *The Development of a New Flame Area Combustion Model Using Conditional Averaging*, Imperial College Mechanical Engineering Department (1993)

[6] H.G. Weller, S. Uslu, A.D. Gosman, R.R. Maly, R. Herweg, B. Heel, *Prediction of Combustion in Homogeneous-Charge Spark-Ignition Engines*, Imperial College Mechanical Engineering Department (1994)

[7] Maurizio Mastropasqua, *Modellazione del processo di combustione in motori Diesel mediante modelli di combustione basati su cinetica chimica tabulata*, Dipartimento di Energia, Politecnico di Milano (2016)

[8] Alberto Comolli, *CFD Modeling of Diesel Combustion with Tabulated Kinetics Based on Homogeneous Reactor Assumption*, Dipartimento di Energia, Politecnico di Milano (2018)

[9] Jiri Vavra, Michal Takats, Vojtech Klir and Marcel Skarohlid, *Influence of Natural Gas Composition on Turbocharged Stoichiometric SI Engine Performances*, Czech Technical Univ. (2012)

[10] Akira Kikusato, Hiroyuki Fukasawa, Kazutoshi Nomura, Jin Kusaka and Yasuhiro Daisho, *A Study on the Characteristics of Natural Gas Combustion at a High Compression Ratio by Using a Rapid Compression and Expansion Machine*, Waseda Univ. (2012)

[11] Ahmed Abdul Moiz, Zainal Abidin, Robert Mitchell, and Michael Kocsis, *Development of a Natural Gas Engine with Diesel Engine-like Efficiency Using Computational Fluid Dynamics*, Southwest Research Institute (2019)

[12] Yalan Liu, Xuexiang Zhang, Junxia Ding, *Chemical effect of NO on CH_4 oxidation during combustion in O_2/NO environments*, University of Chinese Academy of Sciences (2019)

[13] Hrvoje Jasak, *Numerical Solution Algorithms for Compressible Flows*, University of Zagreb, Croatia (2006)

[14] Jinlong Liu and Cosmin Dumitrescu, *CFD Simulation of Metal and Optical Configuration of a Heavy-Duty CI Engine Converted to SI Natural Gas. Part 2: In-Cylinder Flow and Emissions*, West Virginia University (2019)

[15] Fubai Li, Changpeng Liu, Heping Song, and Zhi Wang, *Improving Combustion and Emission Characteristics in Heavy-Duty Natural-Gas Engine by Using Pistons Enhancing Turbulence*, Tsinghua University (2019)

[16] William P. Attard, Elisa Toulson, Harry Watson and Ferenc Hamori, *Abnormal Combustion including Mega Knock in a 60% Downsized Highly Turbocharged PFI Engine*, The University of Melbourne, Australia (2010)

[17] G. Brecq, A. Ramesh, M. Tazerout and O. Le Corre, *An Experimental Study of Knock in a Natural Gas Fuelled Spark Ignition Engine*, Ecole Des Mines De Nantes,(2001)

[18] Junseok Chang, Orgun Güralp, Zoran Filipi, and Dennis Assanis, *New Heat Transfer Correlation for an HCCI Engine Derived from Measurements of Instantaneous Surface Heat Flux*, University of Michigan (2004)

[19] Jeremie Dernotte, John Dec, and Chunsheng Ji, *Investigation of the Sources of Combustion Noise in HCCI Engines*, Sandia National Labs (2014)

[20] Magnus Sjöberg and John E. Dec, Nicholas P. Cernansky, *Potential of Thermal Stratification and Combustion Retard for Reducing Pressure-Rise Rates in HCCI Engines, Based on Multi-Zone Modeling and Experiments*, Sandia National Labs and Mechanical Engineering Department, Drexel University (2005)

[21] Patrick Pertl, Alexander Trattner, Andrea Abis , Stephan Schmidt and Roland Kirchberger, Takaaki Sato *Expansion to Higher Efficiency - Investigations of the Atkinson Cycle in Small Combustion Engines*, Graz University of Technology and DENSO Automotive Deutschland GmbH (2012)

[22] Laura Manofsky, Jiri Vavra, Dennis Assanis and Aristotelis Babajimopoulos *Bridging the Gap between HCCI and SI: Spark-Assisted Compression Ignition*, Univ. of Michigan and Czech Technical Univ (2011)

[23] William P. Attard and Hugh Blaxill, Eric K. Anderson, Paul Litke, *Knock Limit Extension with a Gasoline Fueled Pre-Chamber Jet Igniter in a Modern Vehicle Powertrain*, MAHLE Powertrain, National Research Council and US Air Force Research Laboratory (2012)

[24] Anne Prieur and Richard Tilagone, *A Detailed Well to Wheel Analysis of CNG Compared to Diesel Oil and Gasoline for the French and the European Markets*, IFP (2007)

[25] Chang, J., Kim, M. And Min, K., *Detection of misfire and knock in spark ignition engines by wavelet transform of engine block vibration signals*, Measurement Science and Technology, 2002.

[26] Ohtubo, H., Yamane, K., Kawasaki, K., Nakazono, T. and Shirouzu, T., *PCCI Combustion for Multi Cylinder Natural Gas Engine (Second Report) - Leading Auto-ignition Reduction of Cylinder-to cylinder Variations by using Spark Ignition* JSAE Proceeding Paper, 2007

[27] Roberts, C.E., Snyder, J.C., Stovell, C., Dodge, L.G. et al., *The Heavy-Duty Gasoline Engine-An Alternative to Meet Emissions Standards of Tomorrow* SAE Technical Paper, 2004

[28] Liu, J. and Dumitrescu, C.E., *Combustion Visualization in a Single-Cylinder Heavy-Duty CI Engine Converted to Natural Gas SI Operation*, State College USA, 2018

[29] Yu, X., Liu, Z., Wang, Z., and Dou, H., *Optimize Combustion of Compressed Natural Gas Engine by Improving In-Cylinder Flows* International Journal of Automotive Technology, 2013

[30] Wang, Z., Wang, J., Shuai, S., Tian, G., An, X., and Ma, Q., *Study of the effect of spark ignition on gasoline HCCI combustion*, Journal of Automobile Engineering, 2006.